2019

Microstructural Evaluation of Aluminium Alloy A365 T6 in Machining Operation

Bankole I. Oladapo

S. Abolfazl Zahedi

Francis T. Omigbodun

Edwin A. Oshin
Old Dominion University

Victor A. Adebiyi

See next page for additional authors

Original Publication Citation

Oladapo, B. I., Zahedi, S. A., Omigbodun, F. T., Oshin, E. A., Adebiyi, V. A., & Malachi, O. B. (2019). Microstructural evaluation of aluminium alloy A365 T6 in machining operation. *Journal of Materials Research and Technology, 8*(3), 3213-3222. doi:10.1016/j.jmrt.2019.05.009

Available online at www.sciencedirect.com

jmr&t Journal of Materials Research and Technology

www.jmrt.com.br

Original Article

Microstructural evaluation of aluminium alloy A365 T6 in machining operation

Bankole. I. Oladapo[a,*], S. Abolfazl Zahedi[a], Francis.T. Omigbodun[a], Edwin A. Oshin[b], Victor A. Adebiyi[a], Olaoluwa B. Malachi[c]

[a] School of Engineering and Sustainable Development, De Montfort University, Leicester, UK
[b] Department of Biomedical Engineering, Old Dominion University, Norfolk, Virginia, USA
[c] Computer Science and Engineering, Obafemi Awolowo University, Ile-Ife, Nigeria

ARTICLE INFO

Article history:
Received 18 August 2018
Accepted 7 May 2019

Keywords:
Microstructural
Cutting force
Surface evaluation
Turning operation
Cutting speed

ABSTRACT

The optimum cutting parameters such as cutting depth, feed rate, cutting speed and magnitude of the cutting force for A356 T6 was determined concerning the microstructural detail of the material. Novel test analyses were carried out, which include mechanical evaluation of the materials for density, glass transition temperature, tensile and compression stress, frequency analysis and optimisation as well as the functional analytic behaviour of the samples. The further analytical structure of the particle was performed, evaluating the surface luminance structure and the profile structure. The cross-sectional filter profile of the sample was extracted, and analyses of Firestone curve for the Gaussian filter checking the roughness and waviness profile of the structure on aluminium alloy A356T6 is proposed. A load cell dynamometer was used to measure different parameters with the combination of a conditioning signal system, a data acquisition system and a computer with visualised software. This allowed recording the variations of the main cutting force throughout the mechanised pieces under different cutting parameters. A carbide inserted tool with triangular geometry was used. The result shows that the lowest optimum cutting force is 71.123 N at 75 m/min cutting speed, 0.08 mm/rev feed rate and a 1.0 mm depth of cut. The maximum optimum cutting force for good surface finishing is 274.87 N which must be at a cutting speed of 40 m/min, 0.325 mm/rev feed rate and the same 1.0 mm depth of cut.

1. Introduction

Cutting metals have been the subject of many studies since the 1850s when the industrial revolution was ruined by the development of machining tools such as lathe, drill, milling, brushing and profiling tools. The development of these machines necessitates the investigation of the phenomenon of metal cutting for the manufacture of pieces with different geometries [1,2]. However, it was until the early 1900s that the first studies [3,4] about the behaviour of cutting forces in machining were carried out. The development of new or improved materials to obtain the optimal parameters in the turning process requires the study of the behaviour of the materials when being machined by conventional or automated methods. Turning is a chip-making process widely used for obtaining parts with complex geometry and excellent

* *Corresponding author*. Tel.: +44 (0) 757 046 2847
E-mail: P17243433@my365.dmu.ac.uk (B.I. Oladapo).
https://doi.org/10.1016/j.jmrt.2019.05.009

surface finish required. Materials have now been developed or improved to increase the efficiency of the manufacturing processes to result in a decrease in their weight, desirable aesthetic and mechanical strength [5,6]. This explains why plain steel has been replaced in manufacturing parts in the automotive sector by aluminium alloys such as A356, A357, and A356.2. These have great acceptance in the development of parts for components in the suspension, transmission, body, wheels and engine of vehicles [6,7]. During the turning operation of a piece, three force components are acting on the cutting tool. A force component act in the direction of the longitudinal advancement of the machine (*F*), the second act in the course of the radial advancement of the device (F_d), and the third act in a tangential direction to the surface of the part (F_c) of the components.

The tangential force has a greater magnitude which denominates the main cutting force in the process of turning. It is the force that creates a greater consumption of power due to the high speed of cut in the same direction and its impact on the workpiece [8,9]. Takashi and Shoichi [8] analysed the model to evaluate the effect of the cutter run-out on the cutting force of three-dimensional chip flow in milling as a piling up of the orthogonal cuttings in the planes having the cutting velocities and the chip flow velocities. Paulo and Monteiro [9] presented a study of the correlation between cutting forces and tool wear of polycrystalline diamond (PCD) which is measured when machining a composite A356/20/SiCp-T6. Hu et al. [10] based their research on the analysis of process technology and tool kinematics of high cutting honeycomb composites using a triangular blade, it was designed to be performed by analysing cutting force with ultrasonic and non-ultrasonic assistance. Min et al. [11] researched on the correction of cutting force measurement and impact tests using the dynamometer to measure the cutting forces and transfer function between the measured cutting forces and applied forces, respectively. Guicai and Changsheng [12] and Yuan et al. [13] investigated on tool wear model based on the prediction of the cutting force and the energy consumption on the turning process. Also, it is based on the cutting force estimate using an authenticated force model of the residual surface stress of end milling relating cutting force and temperature. Recently Aezhisai et al. [14] presented their work on the study of the cutting conditions that affect the surface roughness and cutting force relative to the spindle speed, axial, radial depth of cut, feed rate and weight percentage of silicon carbide particle SiC_p but not cutting force control of A356 T6 alloy in turning operations. The focal emphasis of this research work is to optimise and determine the influence of various cutting parameters such as the speed of tool feed rate, cutting depth and cutting speed over the tangential cutting force which is the primary cutting force. To validate the efficiency of this approach, the research reports on:

- An in-depth study of the cutting force control conditions that affect the surface finishing and cutting force relative to the spindle speed, axial, radial depth of cut and feed rate which change the cutting force control of aluminium alloy A356 T6 in turning operations.
- An evaluation of the turning operations of the aluminium alloy A356 T6 using experimental tests performed with a load cell-based dynamometer, a data acquisition module, a signal conditioning system, a personal computer and a conventional lathe commonly found in the Industry.
- To create the mathematical model for cutting force considering the process parameter of spindle speed, feed rate, axial depth of cut, the radial thickness of cut and control force for turning operations of the aluminium alloy A356 T6
- To implement the factor level Design of Experiments (DoE) technique in the measurement of axial and radial cutting force and affect surface finishing in control force for turning operations of the aluminium alloy A356 T6. Although the aluminium alloy A356 is not easily found in the local market which makes the research on the mechanical behaviour of alloy A356 T6 limited in many countries. However, due to the extensive use and acceptance of this alloy in machine parts in the automotive sector, enhanced information on the behaviour of this alloy in machining operations and especially in turning is required.

The parameter in the Daimler Lead Twist Analysis includes a diameter of 40.0 mm, an evaluation length of 2.00 mm and a maximum wavelength of 0.400 mm. Other settings include period length DP (mm), theoretical supply cross-section D_F (μm^2), academic supply cross-section per turn D_{Fu} (μm^2/U), number of threads D_G, contact length in per cent D_{Lu} (%), lead depth D_t (μm) and lead angle D_y (°).

2. Mathematical model of machining tool

According to Refs. [14,15] who developed a model where the cutting force is proportional to the shear strength of the material, the cutting area and the geometry of the tool. These variables were related to a mathematical model. Another simplified model is the specific shear pressure model [14] which proposes to simplify the area of the cutting plane depending on cutting depth, the cutting thickness and the chip. The simplification that is made is that the cutting area is the product of the feed rate (*f*) of the tool and the depth of cut (*d*). According to this model, the cutting force is then obtained by multiplying this simplified cutting area by a factor called the specific shear pressure (K_s), which considers the cutting shears strength of the material:

$$F = K_s \cdot f \cdot d \tag{1}$$

Since the earliest experimental studies on shear forces, many investigations have been carried out presenting equations of the type shown in Eq. (2):

$$F = k \cdot A \cdot f(\emptyset, \alpha, \beta) \tag{2}$$

Several empirical formulas have been proposed but maintaining the original form of Eq. (2). These equations are the product of conditions and parameters such as material characteristics, tool geometry, lubrication, etc. which does not make them applicable to another experiment; although they provide results that serve as a reference for different conditions. In the investigation of Refs. [10–12], an analytical method was developed to leave aside the "particularities" of each test generating

an expression that depends only on the ultimate strength of the material and the cutting area. Kexuan et al. [6] developed a mathematical model for the determination of shear force in machining operations which unlike the theory of specific shear pressure considers the characteristics of the material. The empirical expression is defined as:

$$F_c = 2.11 \cdot S_c \cdot F \cdot d \quad (3)$$

3. Methodology

The material used is a cast aluminium, silicon and magnesium alloy whose designation according to the Aluminum Association (AA) is A356. Four bars were modelled using a model parameter 50.84 mm in diameter and 610 mm long; making a direct casting of the alloy already deduced and balanced in the model conditioned for that purpose. The chemical composition of the model bars was obtained by sampling the rods, and an optical spectrometer was used to obtain the weight per cent of the components. The model bars were subjected to a T6 heat treatment which involves a solubilisation treatment at 540 °C for 4 h followed by rapid cooling in a tub with water at 75 °C for 10 min. After this, an artificial ageing treatment was applied at a temperature of 155 °C for 5 h using a THERMOLYNE model 4800 electric oven. The temperature was controlled by a K-type thermocouple from the oven and

Table 1 – Mechanical properties of the samples tested.

Samples	The module of elasticity (MPa)	Yield strength (0.2% offset of the length calibrated) (MPa)	Ultimate strength (MPa)	Elongation (% by 50 mm)
1	4739.87	128.90	162.16	2.59
2	4855.53	111.67	144.02	1.20
3	4718.44	107.67	164.98	2.25
4	4886.12	112.81	152.93	2.35
Average	4799.99	115.2625	156.0225	2.0975

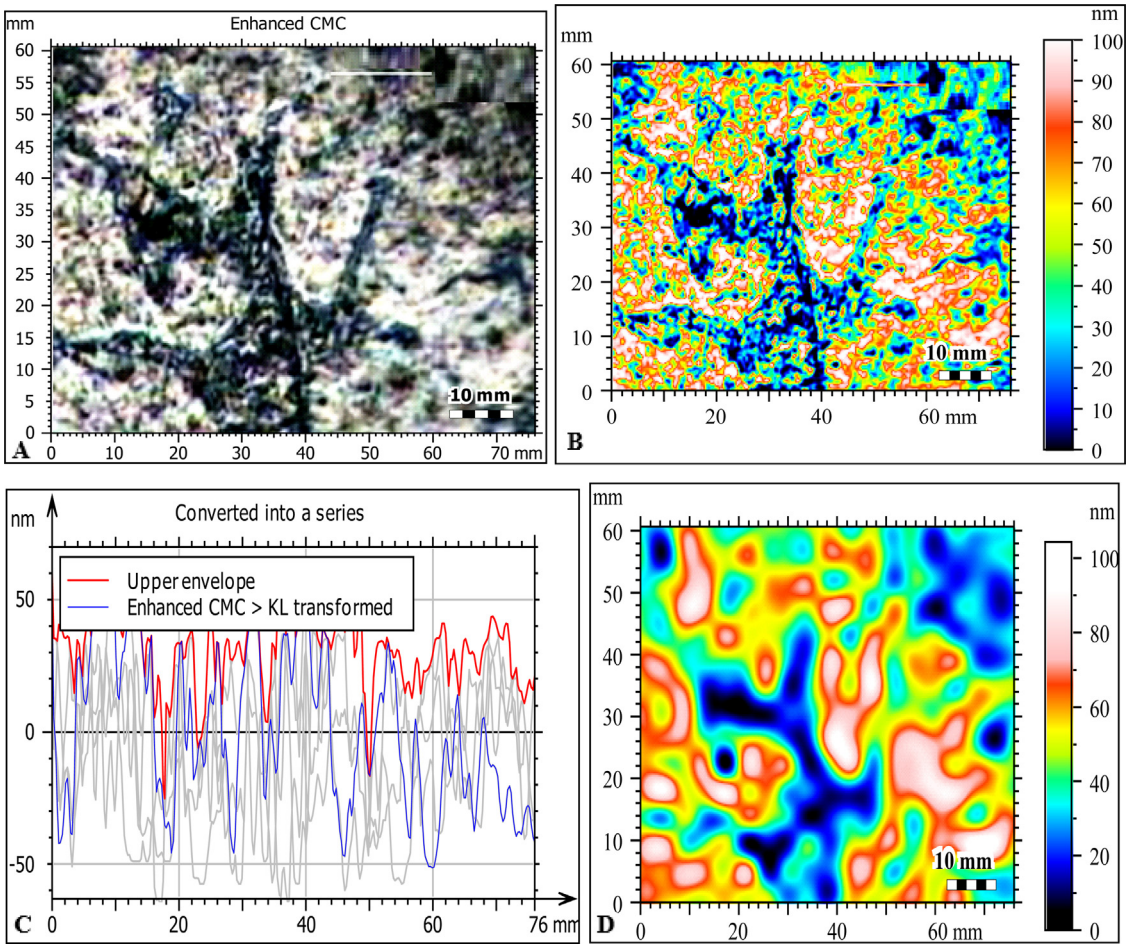

Fig. 1 – Nanostructures of reactive analysis (A) enhance the increase of 100×, (B) surface characterisation of KL transformed in nanometer of the A356 T6 alloy of a Gaussian filter of the materials of the threshold of −60.8 nm to 39.1 nm, (C) surface roughness wavelet filter of the Daubechies 2, and (D) graphical profile of upper enhance KL transformed.

a J-type thermocouple connected to an EXTECH model EX470 digital display [15–17]. The specimens were machined from the heat-treated rods according to ASTM [17,18]. The samples were subjected to a uniaxial tensile test in a Universal GALDABINI Model CTM 20 material test machine with a capacity of 20 metric tonnes, calibrated the length of 50 mm and a test speed of 2 mm/min. This was used to obtain the mechanical properties shown in Table 1 [19]. The hardness measurement of a sample of one of the model bars was taken after the heat treatment (T6) was applied and the surface was prepared according to the recommendations of the ASTM E18 standard [20,21] for measuring Rockwell hardness in metallic materials.

For preparing the sample, the recommendations of ASTM E3 [11] were followed. The recommendations of ASTM E407 [12] were used to develop example by chemical etching, a solution of Tucker 15HF concentration, 45 cc HCL concentration, 15 cc HNO_3 concentration and 70 cc H_3O concentration was used. The prepared sample was observed under a microscope with different magnification scale to obtain the microstructures that are sampled in Fig. 1.

This consists of an enhanced KL converted 2/5 profile with a T-axis and Y-axis of 13.2 mm. The parameters include a length of 76.0 mm, a Pt of 99.9 mm, a scale of 133 mm and a shown scale of 133 nm. The equipment used a signal conditioning system strain gage-based load cell filter with fixed gain. A data acquisition system multifunction data acquisition module connected via USB to a computer system of a power source to power the filter Amplifier which in turn feeds to the load cell with an excitation voltage of 10 V. A personal computer with real-time data visualisation and monitoring software to record the variations of the cutting force along the workpiece. The dynamometer was rectified by applying a known force to the load cell using a universal test machine model CTM 20, then with a digital multimeter. The output voltage the load cell is conditioned by the filter – amplifier. From this, the calibration curve which relates the load applied to the cell, and the already conditioned output voltage by the dynamometer is obtained (Table 2).

The extracted profile of the parameter of the surface characterisation of KL of the A356 T6 alloy was set according to ISO 4287 standard of spacing parameters roughness profile that sooth the experiment. The Gaussian filter was configured to 0.8 mm of a mean width of the roughness profile elements (RSm) of 1.63 mm at root-mean-square slope of the roughness profile (Rdq) 0.000265°. The peak parameters of roughness profile at Gaussian filter of 0.8 mm is of peak count on the roughness profile (RPC) 0.503 L/mm at ±0.5 nm. The material ratio parameters of a primary profile with a relative material ratio of the raw profile (Pmr) of 100% has the highest peak at 1000 nm and a raw profile section height difference (PDC) at 63.7 nm as $p = 20\%$, $q = 80\%$. A relative material ratio of the raw profile (Pmr) of 100% has the highest peak at 3000 nm and raw profile section height difference (Pdc) at 98.1 nm as $p = 2\%$, $q = 98\%$.

The waviness profile information of the analysis includes an appropriate setting of a Gaussian filter with 2.50 nm cut-off,

Table 2 – Parameter of KL transformed of A356 T6 in ISO 25178.

Parameters of Karhunen–Loève theorem (KL) transformed ISO 25178					
Height parameters			Feature parameters		
Root square height (Sq)	29.2 nm		Density of peaks (Spd)	0.123 mm^{-2}	pruning = 5%
Skewness (Ssk)	−0.0315		Arith. peak curvature (Spc)	0.000183 mm^{-1}	pruning = 5%
Kurtosis (Sku)	1.85		Ten point height (S10z)	83.9 nm	pruning = 5%
Peak height (Sp)	49.3 nm		Five peak height (S5p)	42.0 nm	pruning = 5%
Pit height (Sv)	50.7 nm		Five pit height (S5v)	41.9 nm	pruning = 5%
Height (Sz)	100 nm		Mean dale area (SDA)	6.49 mm^2	pruning = 5%
Arithmetic height (Sa)	25.1 nm		Mean hill area (Sha)	6.75 mm^2	pruning = 5%
Functional parameters			3D parameters		
Areal material ratio (Smr)	100%	c = 1000 nm of peak	Mean height absolute (Smean)	129,387,514 nm	
Inverse areal ratio (Smc)	40.5 nm	$p = 10\%$	Developed area (Sdar)	4609 mm^2	
Extreme peak height (Sxp)	49.6 nm	$p = 50\%$ and $q = 97.5\%$	Projected area (Spar)	4609 mm^2	
Spatial parameters			Hybrid parameters		
Autocorrelation (Sal)	3.31 mm	s = 0.2	Root square gradient (Sdq)	5.52e−05	
Texture ratio (Str)	0.728	s = 0.2	Developed interfacial area ratio (Sdr)	1.52e−07%	
Texture direction (Std)	69.7°	Ref. angle = 0°			
Functional parameters volume (mm^3/mm^2)			Functional parameters of stratified surfaces		
Material volume (Vm)	4.78e−07	$p = 10\%$	Core roughness depth (Sk)	4.76 nm	Gaussian filter, 0.8 mm
Void volume (Vv)	4.1e−05	$p = 10\%$	Reduced summit height (Spk)	2.83 nm	Gaussian filter, 0.8 mm
Peak material vol. (Vmp)	4.78e−07	$p = 10\%$	Reduced valley depth (Svk)	3.20 nm	Gaussian filter, 0.8 mm
Core material vol. (Vmc)	3.13e−05	$p = 10\%$ and $q = 80\%$	Root square roughness (Spq)	2.08	Gaussian filter, 0.8 mm
Core void volume (Vvc)	3.87e−05	$p = 10\%$ and $q = 80\%$	Root square roughness (Svq)	11.8	Gaussian filter, 0.8 mm
Pit void volume (Vvv)	2.31e−06	$p = 80\%$	Material ratio valley (Smq)	99.0	Gaussian filter, 0.8 mm

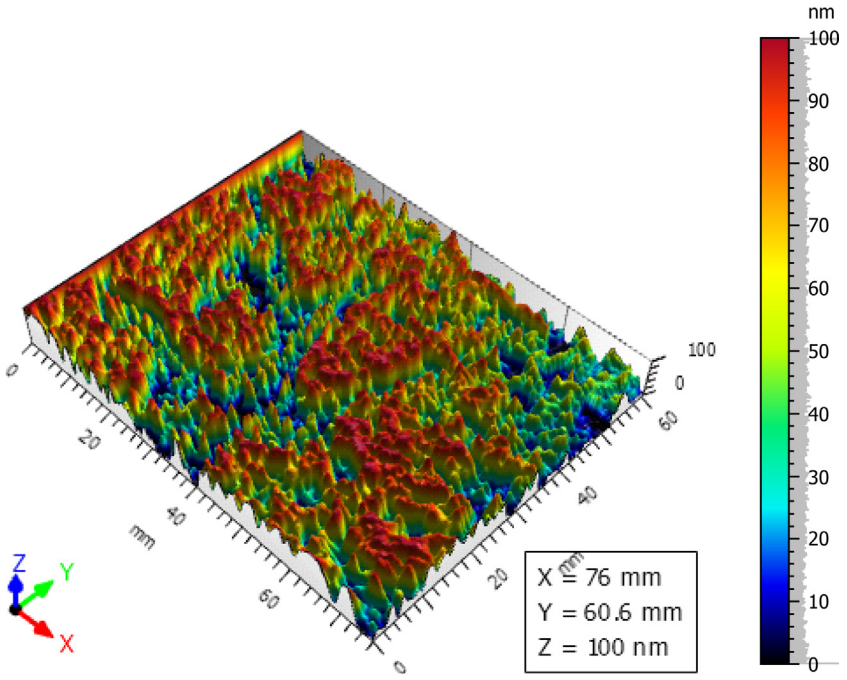

Fig. 2 – Nanostructural 3D view of the surface characterisation of KL transformation of the A356 T6 alloy.

a diameter of 40.0 mm, an evaluation length of 2.00 mm and a maximum wavelength of 0.400 mm. Other parameters include period length DP (mm), theoretical supply cross-section D_F (μm^2), theoretical supply cross-section per turn D_{Fu} (μm^2/U), number of threads DG, contact length in per cent DLC (%), first depth D_t (μm) and lead angle D_y (°).

In the determination of the experimental cutting force, an experimental methodology of machining was designed by combining the cutting parameters and relating them to a $4 \times 4 \times 4$ factorial model. The parameters selected for the machining tests were: 0.06 mm/rev, 0.12 mm/rev, 0.24 mm/rev and 0.38 mm/rev of feed rate, cut depths of 0.25 mm, 0.5 mm, 1.0 mm and 1.5 mm and cutting speeds of 22.97 m/min, 44.07 m/min, 81.40 m/min and 133.0 m/min. The combination of these cutting parameters according to the methodology developed in Section 3 of the research work was used to obtain the shearing force that is generated when turning the alloy A356 T6. The tool position angle was 91°. The machining tests involve external cylindrical specimens made for this purpose using a conventional parallel lathe, a model with bench length of 3 m, turning 40 cm, spindle turning speeds of 50–1200 rpm and positioning accuracy of 0.05 mm. The dimensions of the specimen are 48 mm in diameter and 250 mm in length. The selected turning operation is an external displacement holding the probe with the lathe mandrel on the left side of the bar and placing a counterpoint on the right side of the bar to minimise the effects of buckling and vibrations on the measurements of the cutting force. The cutting depth was constant throughout the machining, and the feed rate was varied in each of the delimited sectors with a constant cutting speed which was also taken as cutting speed average speed considering the diameter of the bar and the speed of rotation of the selected spindle. The machining was done without the use of cutting lubricants. The dynamometer was used for the measurement and recording of the main cutting force for each combination of parameters used in the test. To obtain the average shear force value for each combination of parameters, the data obtained with the use was first analysed. The curve was smoothed using a data post-processing technique called a digital smoothing polynomial filter which smooth the curve by attenuating noise from data acquisition instruments and other sources used. Then the average arithmetic means of the cutting force for the combination of cut parameters tested in the stable zone of the curve was calculated from the data obtained from the smoothed curve (Fig. 2).

4. Discussion of results

The graphs of the cutting force as a function of the experimentally measured cutoff time have a large amplitude due to the characteristics of the load cell used in the dynamometer. The features of the data acquisition module, as well as the variables which occur in the turning process such as the microstructure of the material [21–23] vibrations among other parameters, also have a large amplitude. Smooth experimental curves for each combination of parameters were analysed, determining the average arithmetic mean of the shear force in the stable zone of the curve. In examining the behaviour of the cutting force, it is observed that as the cutting speed increases for a given cut depth, the cutting force decreases slightly. This behaviour of shear strength by increasing the cutting rate was evidenced for almost all combinations of feed rate and sheer depth used in operation as shown in Figs. 4 and 5.

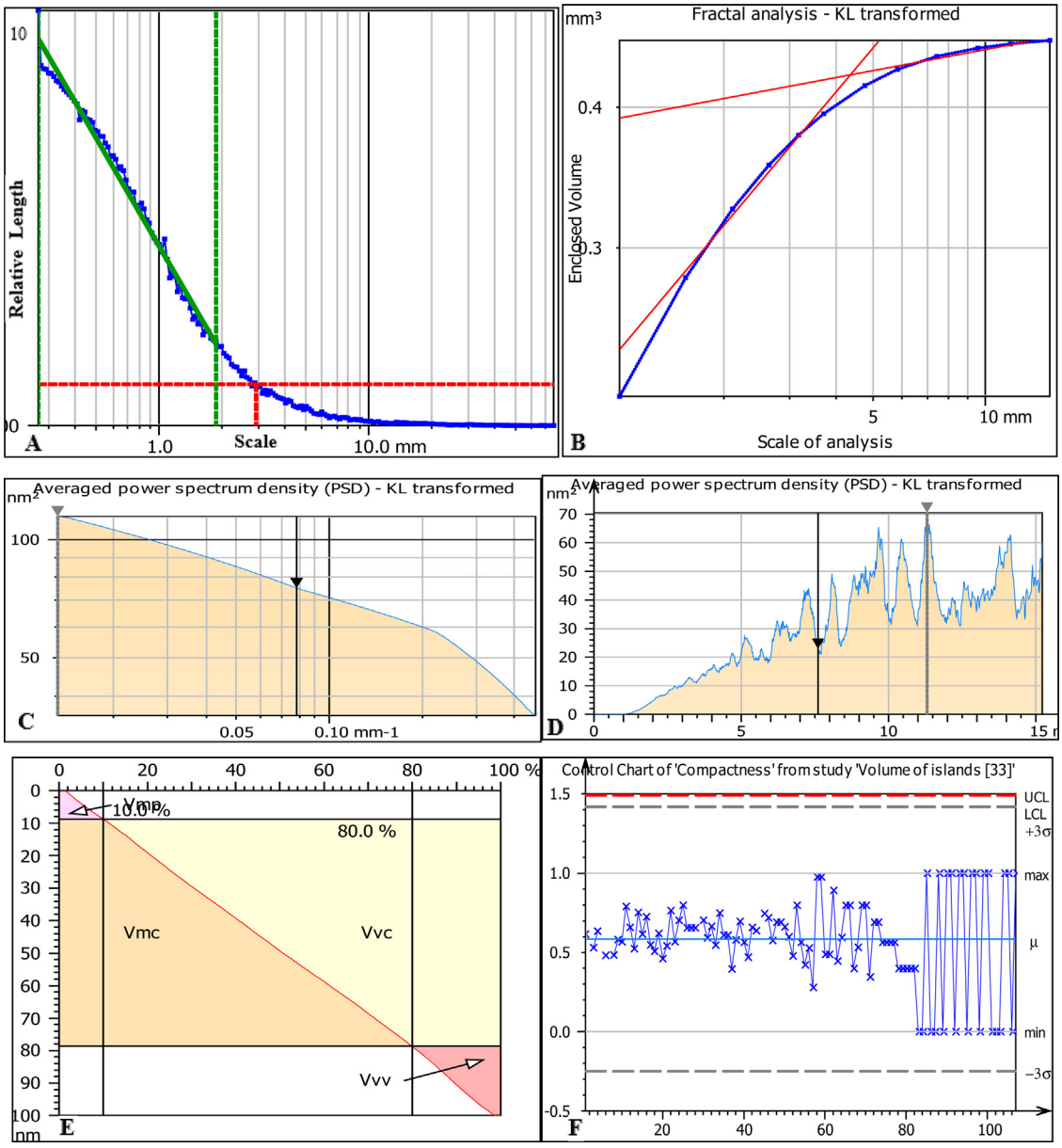

Fig. 3 – Microstructural illustration of the alloy A356 T6: (A) waviness filters of Daubechies 10 characterisation of relative length scale sensitive of surface fractal analysis of KL transformation, (D) complexity of scale sensitivity of fractal analysis of KL transformation, (C and D) averaged power spectrum density of KL transformed, and (E and F) control chart compactness of volumetric parameters of KL transformed.

The alloy A356 T6 waviness filters of Daubechies 10 characterisation of fractal analysis of KL transformation in relative length scale sensitive of surface fractal analysis of KL transformation is represented in Fig. 3A–C. The complexity of scale sensitivity of fractal analysis of KL transformation with the averaged power spectrum density of KL transformed and control chart compactness of volumetric parameters of KL transformed is shown in Fig. 3D–H which has its parameters for Fig. 3D and E and Fig. 3F–H in pairs as follows: projected area 23.6%, 50.8%, volume of void 12.5%, 49.0%, volume of material 87.5%, 51.0%, volume of void 3.116788654e + 12 nm^3/mm^2, 2.452386954e + 13 nm^3/mm^2, volume of material 2.188321078e+13 nm^3/mm^2, 2.54761316e+13 nm^3/mm^2, mean thickness of void 3.12 nm, 24.5 nm, mean thickness of material 21.9 nm, 25.5 nm. The information in Fig. 3 is obtained using morphological envelopes method. The parameters include fractal dimension 2.60, slope (1) 0.397, R^2 (1) 0.989, slope (2) 0.0625 and R^2 (2) 0.937. The information in Fig. 4 is obtained by the length-scale (rows) method with the parameters as follows: number of points 200, Y (Max) 1.00, SRC threshold 1.00, domain max scale 76.0 mm, SRC 2.89 mm, Reg. line slope −2.65e−10, Reg. line Y-intercept 1.32e−10, R^2 0.988,

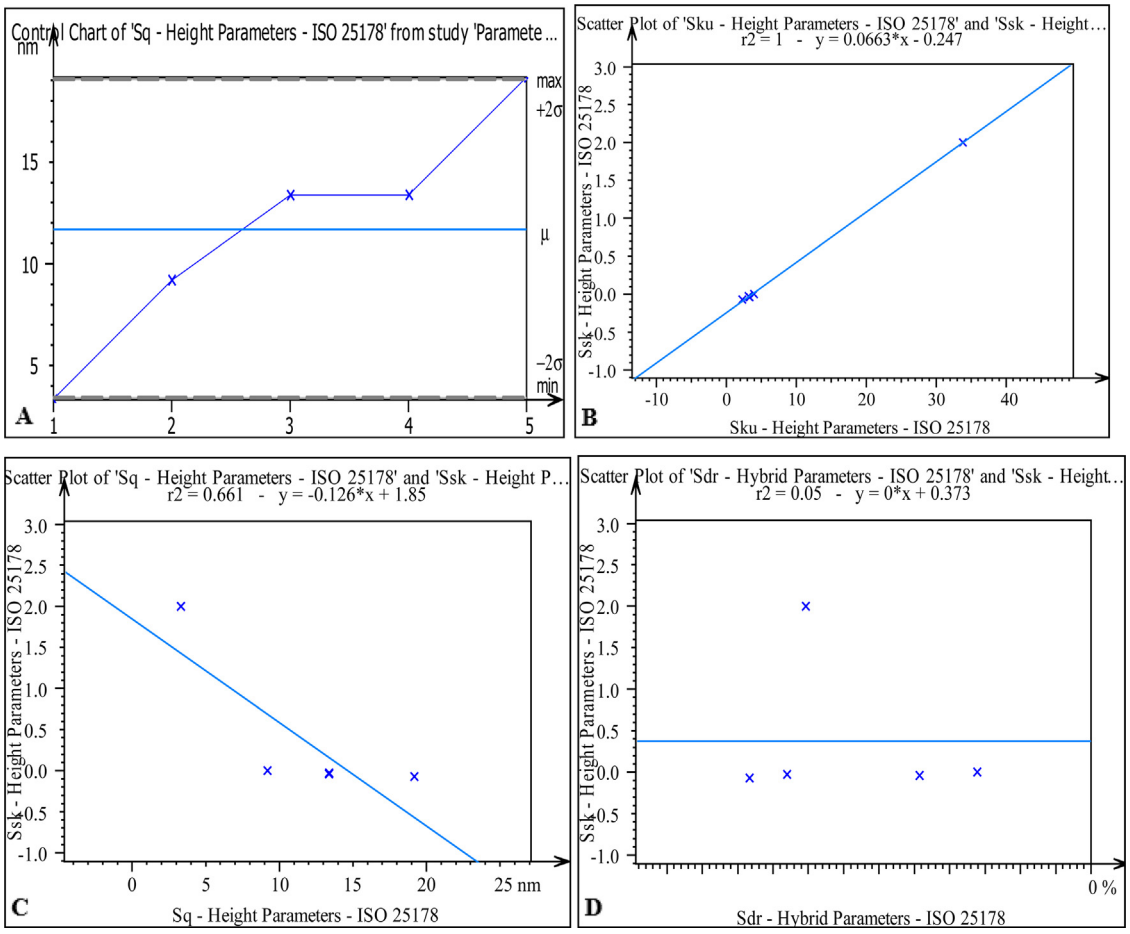

Fig. 4 – Control chart of the sequence of the parameter in ISO 25178: (A) control chart height parameter kurtosis (Sku), (B) scatter plot of skewness (Ssk), (C) parametric root-mean-square height (Sq), and (D) hybrid developed interfacial area ratio.

L_{sfc} 2.65e−07, Dls 1.00, S_{mfc} 0.569 mm and epLsar (1.8 mm, 5°).

The information in Fig. 4 is also obtained by the length-scale method with the following parameters of number of points 200, Y (Max) 1.00, SRC threshold 1.00, domain max scale 76.0 mm, SRC 2.89 mm, Reg. line slope −2.65e−10, Reg. line Y-intercept 1.32e−10, R^2 0.988, L_{sfc} 2.65e−07, Dls 1.00, S_{mfc} 0.569 mm and epLsar (1.8 mm, 5°). The zoom factor information of Fig. 4 is ×4 of a smoothing parameter value with a spatial frequency value of 0.0785 nm^{-1}, an amplitude of 75.2 nm^2, a dominant spatial frequency of 0.0132 nm^{-1} and the maximum amplitude of 114 nm^2. The information represented in Fig. 4 is the zoom factor of ×4 of a smoothing parameter profile with a wavelength of 7.61 mm, an amplitude of 4.79 nm, a dominant wavelength of 11.3 mm and a maximum amplitude of 8.40 nm. It is also and has its parameters as follows as peak material volume (Vmp) 0.000478 ml/m^2, core material volume (Vmc) 0.0313 ml/m^2, core void volume (Vvc) 0.0387 ml/m^2 and pit void volume (Vvv) 0.00231 ml/m^2. It has unfiltered settings with parameters of core roughness depth (Sk) of 97.9 nm, reduce submit height (Spk) of 0.0316 nm, reduce valley depth (Svk) of 2.67 nm, area material ratio (Smr(1)) of 0.0316%, areal material ratio (Smr(2)) of 96.6%, arithmetic mean height (Sa(1)) of 4,991,926 nm^3/mm^2 and arithmetic mean height (Sa(2)) of 4.584235538e + 10 nm^3/mm^2. The parameter's value of Fig. 4 which shows the control chart includes a variance 0.0774^2, yield 0.00%, C_p 24.5, C_{pk} −5.41, C_{pkl} −5.41, C_{pku} 54.4, NT 1.67^2 and ET 40.9^2. Fig. 4 contains information about nanostructure which its parameters include a variance 1678 $(nm/mm^2)^2$, yield 40.2%, C_p 0.166, C_{pk} −0.0367, C_{pkl} 0.369, C_{pku} −0.0367, NT 246 $(nm/mm^2)^2$ and ET 40.9 $(nm/mm^2)^2$. It is the control area of the motif analysis. The parameters are: a variance 229 mm^4, yield 87.7%, C_p 0.450, C_{pk} 0.257, C_{pkl} 0.257, C_{pku} 0.643, NT 90.8 $(mm^2)^2$ and ET 40.9 $(mm^2)^2$.

Fig. 4 represents the control chart of Sq height parameter of the system modification in ISO 25178 standard. The parameters include a variance 27.6 nm^2, yield 80%, C_p 0.524, C_{pk} 0.461, C_{pkl} 0.588, C_{pku} 0.461, NT 31.5 nm^2 and ET 16.5 nm^2. For great tool advancement values, as the cutting speed is increased, the decrease in shear force as compared to low feed rates becomes more noticeable. As the cutting speed is increased for an advance and the cutting depth is increased for a given tool advance, the cutting force required to perform the machining increased. Also, for high cut depth values and grow in the cutting speed, the cutting strength decreases in

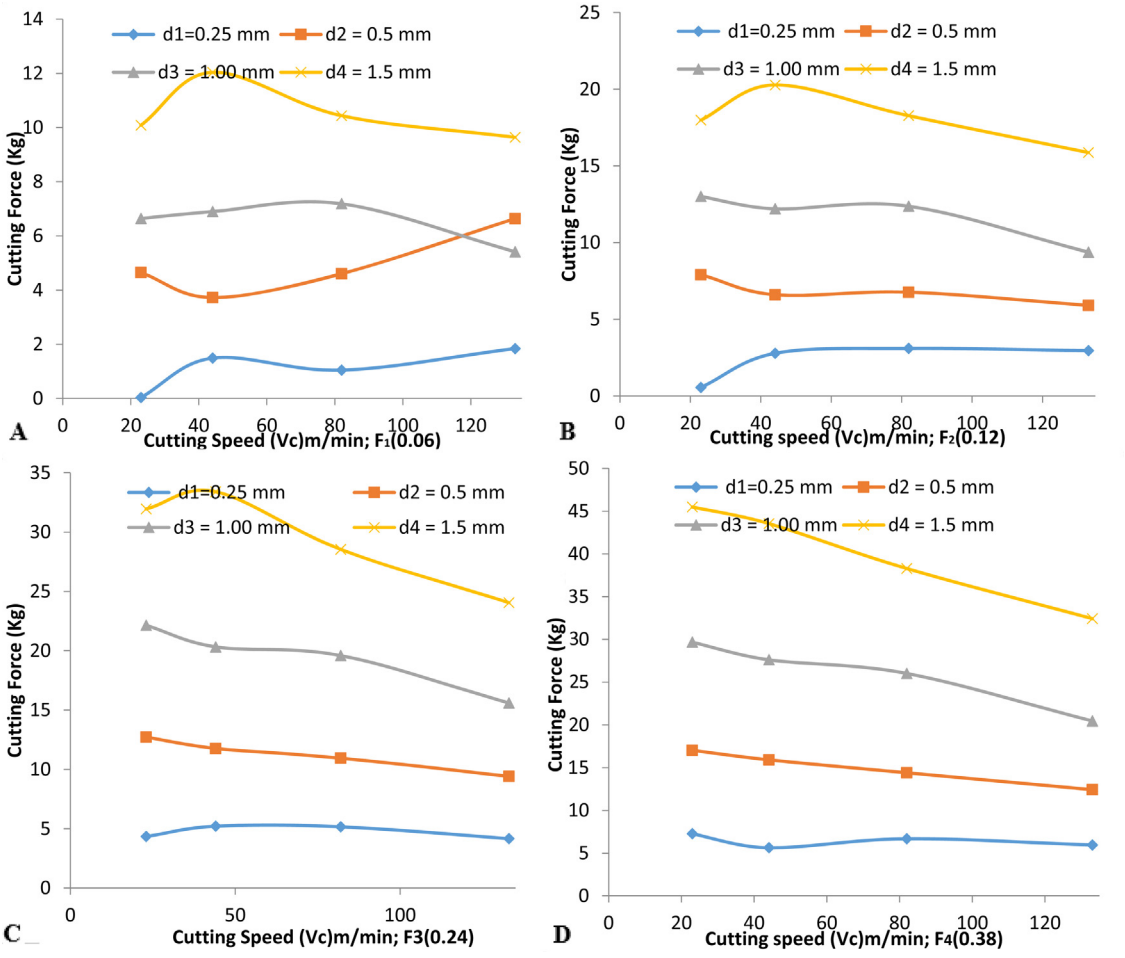

Fig. 5 – Cutting force against cutting speed (Vc) m/min at different depths of cut (D) for the four-cutting speed.

comparison to low cut depth values as shown in Figs. 5 and 6. For a feed rate used, the behaviour is like the rest of the feed rate.

As the cutting depth is increased for constant cutting speed, the required cutting force is linearly increased because the cutting area increased, and more material is removed per unit time. This behaviour was evidenced by the full range of feed rate used in the graph as shown in Fig. 4. As the feed rate of the tool increased to a constant depth of cut, the required cutting force is linearly increased because the cutting area also improved and more material is removed per unit time. This behaviour was evidenced by the full range of shear rates used in the tests as shown in Fig. 5. As the cutting depth is increased for constant cutting speed, the required cutting force is linearly increased because the cutting area also improved and more material is removed per unit time. This behaviour was evidenced by the entire range of tool advances used in the tests as shown in Fig. 6.

As the depth of cut for a constant tool advance increases, the cutting force required is linearly increased. This is because the cutting area also improved and more materials are removed per unit time. This behaviour was evidenced by the full range of feed rate used in the tests as shown in Fig. 6. The optimal levels for the turning of aluminium alloy A356 T6 in centre lathe to obtain minimum surface roughness and cutting force of 71.123 N at 75 m/min cutting speed are at a feed rate of 0.08 mm/rev and 1.0 mm depth of cut. The maximum optimum cutting force for good surface finishing is 274.8762 N which must be at a cutting speed of 40 m/min of 0.325 mm/rev feed rate and the same 1.0 mm depth of cut which are the measured optimal parameters for the turning operations of aluminium alloy A356 T6.

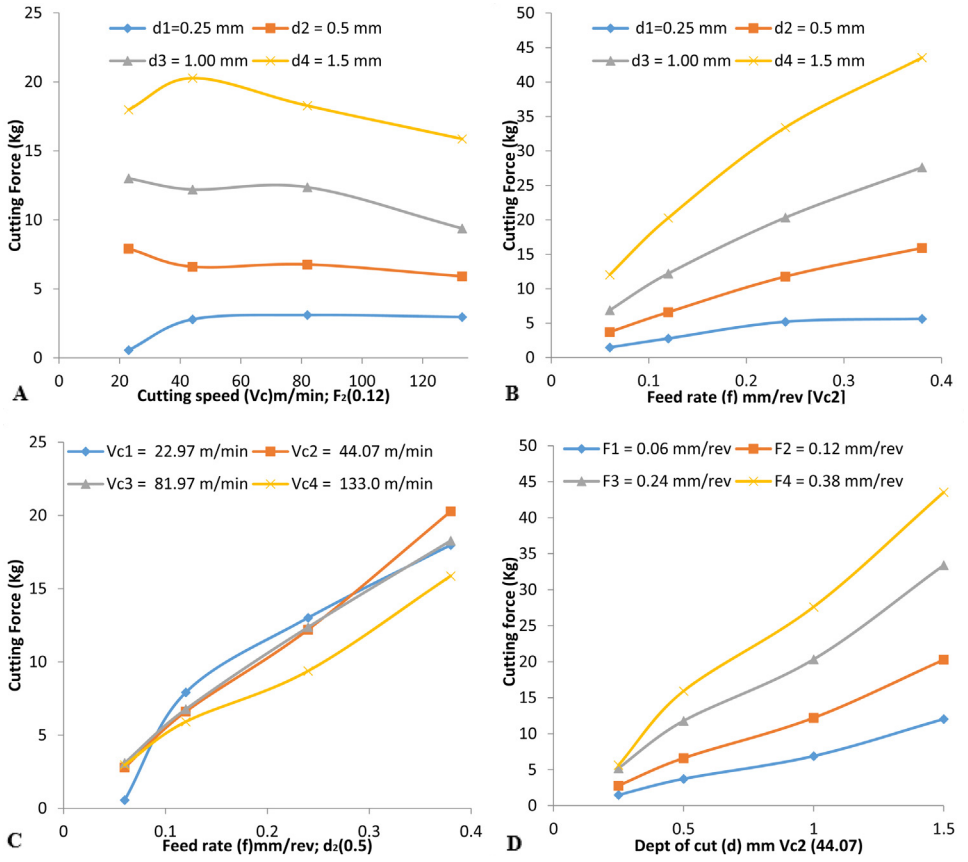

Fig. 6 – Four different operating cutting force against (A) cutting speed (Vc) m/min to varying depths of cut, (B) feed rate (*f*) mm/rev, (C) feed rate (mm/rev) at different cutting speed (Vc), (D) depths of cut (*d*) mm at a different feed rate.

5. Conclusions

The main cutting force was measured and recorded experimentally in turning operation of the aluminium alloy A356 T6. It was discovered that as the cutting speed in the turning of A356 T6 alloy increases, the cutting force required to perform the turning operation to maximum satisfaction is slightly reduced. As the feed rate or cutting depth of the tool increases, the cutting area in the turning of A356 T6 alloy increases, it also increases the cutting force required to perform the machining operation to optimal satisfaction. This research proposes a novel evaluation for the possible turning of A356 T6 alloy of different sample and examine it nanoparticles and microstructural behaviour to enhance productivities. According to the results obtained in the tensile and compression tests, the resistance of the A356 T6 alloy was low when compared to the other commercial alloy, but they presented fair values if the desired application was treated according to the results obtained in differential scanning calorimetry and the analysis of the microstructure. The resins showed different behaviour from the low-temperature state to the high-temperature state, which is typical of crystalline and semi-crystalline alloy, with characteristics like the industrial plastics. The maximum shear force measured in the experimental tests was 45.50 kg for the following combination of parameters: cutting speed of 22.97 m/min, a feed rate of 0.35 mm/rev and cutting depth of 1.50 mm. The alloy presented different thermoplastic behaviour, and the values concerning the contraction and expansion of these materials were evaluated, as well as its compatibility and emissions of compounds when subjected to heating processes. Also, such as those occurring in the cast-deposition this study opens the way for other researches regarding the identification of the characteristics of another alloy available for application in cutting operation.

Funding

This project is funded by the Higher Education Innovation Fund (HEIF) of De Montfort University 2017-2018, UK: Research Project No.0043.06

Conflicts of interest

The authors declare no conflicts of interest.

REFERENCES

[1] Tukora B, Szalay T. Real-time determination of cutting force coefficients without cutting geometry restriction. IJMTM 2011;51(12):871–9.

[2] Denkena B, Vehmeyer J, Niederwestberg D, Maaß P. Identification of the specific cutting force for geometrically defined cutting edges and varying cutting conditions. Int J. Mach Tool Manu 2014;82-83:42–9.
[3] Cha W-G, Hammer T, Gutknecht F, Golle R, Tekkaya AE, Volk W. Adaptive wear model for shear-cutting simulation with the open cutting line. Wear 2017;386–387(15):17–28.
[4] Zahedi SA. Crystal-plasticity modelling of machining. PhD thesis; 2014.
[5] Bankole I, Oladapo SA, Zahedi AO, Awe FT, Omigbodun VA, Adebiyi. Analysis on corrosion resistant of electrodeposited ternary Co–W–P alloy. Appl Surf Sci 1 May 2019;475:627–32.
[6] Zahedi SA, Demirel M, Roy A, Silberschmidt VV. FE/SPH modelling of orthogonal micro-machining of fcc single crystal. Comput Mater Sci 2013;78:104–9.
[7] Wan M, Pan W-J, Zhang W-H, Ma Y-C, Yang Y. A unified instantaneous cutting force model for flat end mills with variable geometries. JMPT 2014;214(3):641–50.
[8] Takashi M, Shoichi T. Cutting force model in milling with cutter run out. Procedia CIRP 2017;58:566–71.
[9] Zahedi SA, Roy A, Silberschmidt VV. Modeling of micro-machining single-crystal fcc metals. Procedia CIRP 2013;8:346–50.
[10] Zahedi SA, Li S, Roy A, Babitsky V, Silberschmidt VV. Application of smooth-particle hydrodynamics in metal machining. J Phys: Conf Ser 2012;382(1):012017.
[11] Wan M, Yin W, Zhang W. Study on the correction of cutting force measurement with table dynamometer. Procedia CIRP 2016;(56):119–23.
[12] Oladapo BI, Adeoye AOM, Ismail M. Analytical optimisation of a nanoparticle of microstructural fused deposition of resins for additive manufacturing. Compos Part B: Eng 2018;150(1):248–54.
[13] Ma Y, Feng P, Zhang J, Wu Z, Yu D. Prediction of surface residual stress after end milling based on cutting force and temp. J Mater Process Technol 2016;(235):41–8.
[14] Ijagbemi CO, Oladapo BI, Campbell HM, Ijagbemi CO. Design and simulation of fatigue analysis for a vehicle suspension system (VSS) and its effect on global warming. Procedia Eng 2016;159:124–32.
[15] Liu G, Wang Q, Liu T, Ye B, Jiang H, Ding W. Effect of T6 heat treatment on microstructure and mechanical property of 6101/A356 bimetal fabricated by squeeze casting. Mater Sci Eng 2017;(696):208–15.
[16] Houria MB, Nadot Y, Fathallah R, Roy M, Maijer DM. Influence of casting defect and SDAS on the multiaxial fatigue behavior of A356-T6 alloy including mean stress effect. IJF 2015;(80):90–102.
[17] Buchkremer S, Klocke F. Compilation of a thermodynamics-based process signature for the formation of residual surface stresses in metal cutting. Wear 2017;376-377(B):1156–63.
[18] Adeoye AOM, Kayode JF, Oladapo BI, Afolabi SO. Experimental analysis and optimization of synthesized magnetic nanoparticles coated with PMAMPC-MNPs for bioengineering application. St. Petersburg Polytech Univ J: Phys Math 2017 December;3(4):333–8.
[19] Pham T-H, Kim S-R. Determination of equi-biaxial residual stress and plastic properties in structural steel using instrumented indentation. Mater Sci Eng A 2017;688(14):352–63.
[20] Samuel O, Afolabi, Bankole I, Oladapo, Christianah O, Ijagbemi, Adeyinka OM, Adeoye, Joseph F, Kayode. Design and finite element analysis of a fatigue life prediction for safe and economical machine shaft. J Mater Res Technol 2019;8(1):105–11.
[21] Kushner V, Storchak M. Determination of material resistance characteristics in cutting. Procedia CIRP 2017;58:293–8.
[22] Oladapo BI, Zahedi SA, Adeoye AOM. 3D printing of bone scaffolds with hybrid biomaterials. Compos Part B: Eng 1 February 2019;158:428–36.
[23] Wan M, Zhang W, Dang J, Yang Y. A novel cutting force modelling method for cylindrical end mill. Appl Math Model 2010;34:823–36.